

This is an Open Access document downloaded from ORCA, Cardiff University's institutional repository: <https://orca.cardiff.ac.uk/id/eprint/136608/>

This is the author's version of a work that was submitted to / accepted for publication.

Citation for final published version:

Field, Daniel E., Cuenca, Jerome A. , Smith, Matthew, Fairclough, Simon M., Massabuau, Fabien C-P., Pomeroy, James W., Williams, Oliver , Oliver, Rachel A., Thayne, Iain and Kuball, Martin 2020. Crystalline interlayers for reducing the effective thermal boundary resistance in GaN-on-Diamond. ACS Applied Materials and Interfaces 12 (48) , pp. 54138-54145. 10.1021/acsami.0c10129

Publishers page: <http://dx.doi.org/10.1021/acsami.0c10129>

Please note:

Changes made as a result of publishing processes such as copy-editing, formatting and page numbers may not be reflected in this version. For the definitive version of this publication, please refer to the published source. You are advised to consult the publisher's version if you wish to cite this paper.

This version is being made available in accordance with publisher policies. See <http://orca.cf.ac.uk/policies.html> for usage policies. Copyright and moral rights for publications made available in ORCA are retained by the copyright holders.



# Crystalline interlayers for reducing the effective thermal boundary resistance in GaN-on-diamond

*Daniel E. Field<sup>1,2</sup>, Jerome A. Cuenca<sup>3</sup>, Matthew Smith<sup>4</sup>, Simon M. Fairclough<sup>5</sup>, Fabien C-P. Massabuau<sup>5,6</sup>, James W. Pomeroy<sup>1</sup>, Oliver Williams<sup>3</sup>, Rachel A. Oliver<sup>5</sup>, Iain Thayne<sup>4</sup>, Martin Kuball<sup>1</sup>.*

*<sup>1</sup>Centre for Device Thermography and Reliability, H.H. Wills Physics Laboratory, University of Bristol, Bristol, BS8 1TL, United Kingdom; <sup>2</sup>Centre for Diamond Science and Technology, University of Warwick, Coventry, CV4 7AL, United Kingdom; <sup>3</sup>Diamond Foundry, School of Physics and Astronomy, University of Cardiff, Cardiff, CF24 3AA, United Kingdom; <sup>4</sup>James Watt School of Engineering, University of Glasgow, Glasgow, G12 8QQ, United Kingdom; <sup>5</sup>Cambridge Centre for Gallium Nitride, Department of materials science and metallurgy, University of Cambridge, Cambridge, CB3 0FS, United Kingdom; <sup>6</sup>Department of Physics, SUPA, University of Strathclyde, Glasgow, G1 1XQ, United Kingdom.*

KEYWORDS: GaN-on-Diamond, Thermal Boundary Resistance, Thermal Management, GaN, Diamond, SiC, AlGaIn, AlN

## ABSTRACT

Integrating diamond with GaN high electron mobility transistors (HEMTs) improves thermal management, ultimately increasing the reliability and performance of high-power high-frequency

RF amplifiers. Conventionally, an amorphous interlayer is used before growing polycrystalline diamond onto the GaN in these devices. This layer contributes significantly to the effective thermal boundary resistance ( $TBR_{\text{eff}}$ ) between the GaN HEMT and the diamond, reducing the benefit of the diamond heat spreader. Replacing the amorphous interlayer with a higher thermal conductivity crystalline material would reduce  $TBR_{\text{eff}}$  and help to enable the full potential of GaN-on-diamond devices. In this work, a crystalline  $\text{Al}_{0.32}\text{Ga}_{0.68}\text{N}$  interlayer has been integrated into a GaN/AlGaN HEMT device epitaxy. Two samples were studied, one with diamond grown directly on the AlGaN interlayer and another incorporating a thin crystalline SiC layer between the AlGaN and diamond. The  $TBR_{\text{eff}}$ , measured using transient thermoreflectance, was improved for the sample with SiC ( $30 \pm 5 \text{ m}^2 \text{ K GW}^{-1}$ ) compared to the sample without ( $107 \pm 44 \text{ m}^2 \text{ K GW}^{-1}$ ). The reduced  $TBR_{\text{eff}}$  is thought to arise from improved adhesion between the SiC and the diamond compared to the diamond directly on the AlGaN due to an increased propensity for carbide bond formation between SiC and diamond. The stronger carbide bonds aid transmission of phonons across the interface, improving heat transport.

## INTRODUCTION

Gallium nitride (GaN) based high electron mobility transistors (HEMTs) are promising devices for high-frequency, high-power amplifiers required for the next generation of communication technologies<sup>1</sup>. These devices have excellent electrical properties such as high electron mobilities, high saturation velocities, and high breakdown fields. These result from the intrinsic material properties of GaN and the formation of a two-dimensional electron gas at the AlGaN/GaN heterojunction interface. AlGaN/GaN HEMTs have been demonstrated operating at  $20 \text{ W mm}^{-1}$  in the X-band<sup>2</sup>. However, thermal management limits device performance; highly localized Joule

self-heating at the drain edge of the gate degrades device reliability and performance<sup>3</sup>. As a result, the devices used in commercial applications are often significantly de-rated with respect to the highest reported power densities<sup>1</sup>.

Devices fabricated on SiC substrates have improved high-power reliability and performance compared to devices on Si and sapphire substrates. This is a result of SiC's much higher thermal conductivity of  $\sim 400 \text{ W m}^{-1} \text{ K}^{-1}$ <sup>4</sup> compared to Si ( $130 \text{ W m}^{-1} \text{ K}^{-1}$ <sup>5</sup>) and sapphire ( $40 \text{ W m}^{-1} \text{ K}^{-1}$ <sup>6</sup>) at room temperature. Despite this, the output power density (or device lifetime) of GaN-on-SiC HEMTs is still limited by their thermal management. Diamond has the highest known bulk thermal conductivity ( $>2000 \text{ W m}^{-1} \text{ K}^{-1}$  at room temperature<sup>7</sup>). Several GaN/diamond integration methods have been pursued for improved thermal management<sup>8-12</sup>: overgrowth of a diamond heat spreader onto a device<sup>8</sup>; GaN growth on a diamond substrate<sup>9</sup>; low temperature bonding of diamond wafers to GaN<sup>10</sup>. By far the most successful integration method begins with the removal of the growth substrate, typically Si, and strain relief layers (SRL), followed by polycrystalline diamond growth by microwave plasma chemical vapor deposition (MWCVD) onto the GaN backside<sup>11,12</sup>. It is imperative to minimize the thermal resistance between the GaN channel and diamond. If the thermal resistance between the GaN and diamond is too large, this thermal bottleneck can negate any benefit from using a high thermal conductivity diamond heat spreader<sup>11</sup>. A seeding interlayer, such as amorphous  $\text{SiN}_x$ , is typically deposited onto the GaN. The  $\text{SiN}_x$  has two purposes, to adhere the diamond and to protect the GaN from the harsh environment in the diamond growth reactor ( $\text{H}_2$  plasma,  $>700^\circ\text{C}$ ). The thermal conductivity of this interlayer, the thermal conductivity of the diamond near to the nucleation layer (a result of the gradient in thermal conductivity of polycrystalline diamond<sup>13</sup>), and the strength of the interfacial bond are the biggest contributions

to the thermal resistance across the GaN/diamond interface. The effective thermal boundary resistance ( $TBR_{\text{eff}}$ ) is a lumped term including all these contributions.

To maximize the benefit of using diamond heat sinks placed close to the transistor channel, the  $TBR_{\text{eff}}$  must be minimized. The thermal conductivity of the amorphous  $\text{SiN}_x$  interlayer is very low, around  $1\text{-}2\text{ W m}^{-1}\text{ K}^{-1}$ <sup>14</sup>, so generally  $TBR_{\text{eff}}$  reduction has been achieved by making this interlayer as thin as possible. However, if too thin, the harsh diamond growth conditions can etch pinholes into the GaN<sup>15</sup>. Recently we have reported on the use of crystalline AlN as a seed layer for diamond growth resulting in a  $TBR_{\text{eff}}$  as low as  $16\text{ m}^2\text{ K GW}^{-1}$ , compared to typical values seen for  $\text{SiN}_x$  of  $\sim 20\text{-}25\text{ m}^2\text{ K GW}^{-1}$ <sup>16,17</sup>. This is due to the high thermal conductivity of bulk AlN,  $\sim 285\text{ W m}^{-1}\text{ K}^{-1}$ <sup>18</sup>, and good adhesion to the diamond. Earlier reports of direct diamond deposition onto GaN have shown that, while depositing thin ( $\sim 1\text{ }\mu\text{m}$ ) diamond layers is possible they are not strongly adhered and thicker films delaminate<sup>19</sup>. This is likely due to the lack of strong carbide bonds at the interface. Ideally, a crystalline AlN interlayer would be integrated into the device epitaxy, just below the GaN channel<sup>20</sup>. This layer would act as an etch stop, allowing selective etching of the SRL and part of the GaN buffer layer without damaging the GaN channel, as well as a seed layer for subsequent diamond growth<sup>21</sup>. However, integration of thin AlN or high Al content AlGaIn layers at this point in the epitaxy is challenging due to alloying with surrounding layers. As a result of these issues, in this work a relatively low Al content crystalline  $\text{Al}_{0.32}\text{Ga}_{0.68}\text{N}$  layer is used as the etch stop and interlayer. We demonstrate in this letter that whilst a direct growth on this layer results in a relatively high  $TBR_{\text{eff}}$ , this can be much improved by depositing a thin crystalline SiC layer in between the diamond and the  $\text{Al}_{0.32}\text{Ga}_{0.68}\text{N}$  layer.

## EXPERIMENTAL METHODS

AlGaIn/GaN-on-Si high electron mobility transistor structures were grown by metal organic chemical vapor deposition (MOCVD) with typical AlGaIn strain relief layer (SRL). The samples were obtained commercially, and full growth details are not available. An additional ~20 nm thick  $\text{Al}_{0.32}\text{Ga}_{0.68}\text{N}$  etch stop layer was introduced during growth within the GaN buffer layer, 750 nm below the AlGaIn/GaN channel. Two samples were prepared: 1) the structure was inverted via a substrate transfer process, with the original top surface being attached to a Si handle wafer using spin-on-glass (SOG) and polycrystalline Si, followed by removal of the original Si substrate using chemical-mechanical lapping and reactive ion etching (RIE) processes<sup>12,22</sup>, from now on referred to as Sample 1; 2) a membrane based technique<sup>23</sup> was used to selectively remove small areas ( $\varnothing$  0.5 mm) of the Si substrate, effectively forming GaN membranes, using a Bosch process, denoted in the following as Sample 2. After removing the Si substrate for both Samples 1 and 2, a two-stage dry etching process was used to reveal the AlGaIn etch stop. Initially, a high power  $\text{Cl}_2/\text{Ar}$  inductively coupled plasma (ICP) etch removed the majority of the SRL and GaN buffer. This process is fully described in ref.<sup>21</sup>. The final ~200 nm of GaN buffer was removed by a  $\text{Cl}_2/\text{N}_2/\text{O}_2$  ICP etch process, chosen for its AlGaIn/GaN etch rate selectivity with a reduced power in order to prevent damage to the III-nitride material<sup>24</sup>.

Diamond was grown on the backside of Samples 1 and 2 using a process similar to growth on crystalline AlN; both samples were exposed to a  $\text{N}_2/\text{H}_2$  plasma flash (1.5 kW at 20 Torr with  $\text{N}_2$  concentration at 10% in a total flow rate of 300 sccm) for 10 minutes before seeding<sup>16</sup>. Owing to the fragility of the membranes, conventional ultrasonic seeding was not used and instead drop cast seeding of a suspension of oxygen terminated detonation nanodiamond was carried out. Diamond growth was then carried out by MWCVD in a  $\text{CH}_4/\text{H}_2$  plasma at approximately 800°C (5.5 kW at 110 to 120 Torr with  $\text{CH}_4$  concentration at 3% in a total flow rate of 500 sccm), following the

method in Ref <sup>16</sup>. The diamond film of Sample 2 is ~35  $\mu\text{m}$ -thick, whilst a thinner film was grown for the Sample 1 ( $<1\ \mu\text{m}$ ). Unetched areas of Sample 2's Si substrate, outside the membranes, were sputtered by the  $\text{H}_2$  plasma in the diamond growth reactor and deposited onto exposed areas of the AlGaN layer; this provides a silicon source for SiC formation in the initial stages of diamond growth. Sample 1 on the other hand had no exposed Si surfaces during diamond growth, meaning that SiC could not form between the AlGaN and the diamond. The sample structures are depicted in Fig. 1.

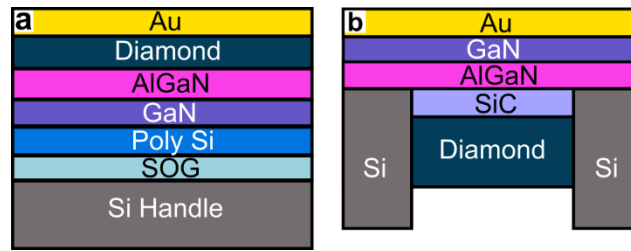


**Figure 1.** Schematic structures of Sample 1 (a) and Sample 2 (b) following diamond growth and transducer deposition

Scanning transmission electron microscopy (STEM) and energy dispersive x-ray spectroscopy (EDS) was used to characterize the samples. TEM cross sections were prepared using a FEI Helios Focus Ion Beam milling with a Ga ion beam. Samples were imaged in a FEI Osiris microscope running at 200 kV and at a beam current of 80 pA or an FEI Titan G2 running at 300 kV at a beam current of 80 pA. EDS were taken using the SuperX EDS system utilizing 4 EDS detectors. All data was analyzed using HyperSpy and the relative compositions determined using Cliff-Lorime k-factors.

The samples were coated by thermal evaporation with 145 nm of Au on a 10 nm Cr adhesion layer, used as a transducer for transient thermoreflectance (TTR) measurements. On Sample 1, the metal was deposited on the diamond, whilst on Sample 2 it was deposited on the GaN (Fig. 1). A

532 nm probe laser (spot size  $\sim 2 \mu\text{m}$ ) was used to monitor the reflectivity of the Au surface whilst a 355 nm ns-pulsed pump laser (spot size  $\sim 85 \mu\text{m}$ ) was used to periodically heat the sample surface<sup>25</sup>. The change in reflectivity of the surface is directly proportional to the temperature change. This means the reflected intensity tracks the temperature change of the surface and the normalized reflected intensity is equal to the normalized surface temperature change. By fixing the known material properties, shown in Table 1, it is possible to obtain  $\text{TBR}_{\text{eff}}$  between the diamond and the GaN by adjusting this as a fitting parameter. Fitting was carried out with an adapted least squares global search algorithm<sup>26</sup>. It was also necessary to fit the thermal boundary resistance (TBR) between the transducer and the first layer for both samples and the thickness of the diamond for Sample 1 between the limits of 500 nm to 1  $\mu\text{m}$ .

**Table 1.** Material properties (in and out of plane thermal conductivity, density, and specific heat) used to solve the heat diffusion equations for fitting the TTR experimental data.

	$\kappa_{\perp}$ ( $\text{W m}^{-1} \text{K}^{-1}$ )	$\kappa_{\parallel}$ ( $\text{W m}^{-1} \text{K}^{-1}$ )	$\rho$ ( $\text{Kg m}^{-3}$ )	$c_p$ ( $\text{J Kg}^{-1} \text{K}^{-1}$ )
Au	317 <sup>27</sup>	Isotropic	19320 <sup>28</sup>	128 <sup>28</sup>
GaN	130 <sup>29</sup>	Isotropic	6150 <sup>28</sup>	490 <sup>30</sup>
Diamond Near Nucleation	350 <sup>13</sup>	150 <sup>13</sup>	3515 <sup>28</sup>	520 <sup>31</sup>
Diamond Bulk	1500 <sup>13</sup>	1000 <sup>13</sup>		
Poly Si	25 <sup>32</sup>	Isotropic	2320 <sup>33</sup>	700* <sup>34</sup>
Spin-on-glass <sup>†</sup>	1.4 <sup>35</sup>	Isotropic	2200 <sup>28</sup>	1000 <sup>35</sup>

\*Heat capacity used of bulk Si. <sup>†</sup>Spin-on-glass properties used were those of silicon dioxide. Parameters are all given at 300 K with no temperature dependence assumed.

In addition to this experimental work, simulations were undertaken to estimate a theoretical minimum limit for  $\text{TBR}_{\text{eff}}$ , called here  $\text{TBR}_{\text{interlayer}}$ , for SiC, AlN, and  $\text{Al}_x\text{Ga}_{(1-x)}\text{N}$  interlayers. This value has been determined by summing the TBR of the two interfaces present (GaN-interlayer, and interlayer-diamond), and the thermal resistance associated with heat conduction through the

interlayer. The thermal resistance within the interlayer was calculated by first calculating the cross-plane thermal conductivity of thin films of the layer using the grey approximation, *i.e.*, taking a single, mode-independent phonon velocity and phonon lifetime and using the Matthiessen rule for diffuse boundary scattering<sup>36</sup>. This allows for calculation of a thin film's thermal conductivity as a function of its bulk thermal conductivity and the film thickness<sup>37</sup>. For more detail, the reader is referred to refs<sup>35</sup> and<sup>36</sup>. The thermal resistance of the film is then given by the film thickness divided by its thermal conductivity. The TBR of the different interfaces was calculated using the diffuse mismatch model (DMM)<sup>38</sup>. In each case, the interface is assumed to be perfectly adhered and neglects the contribution of the near nucleation diamond to  $TBR_{eff}$ , *i.e.*  $TBR_{interlayer}$  is a predicted lower limit value for  $TBR_{eff}$ . The material properties used for these calculations are shown in Table 2. For  $Al_xGa_{(1-x)}N$ , these were calculated using the procedure set out in ref<sup>39</sup> using the bulk properties of AlN and GaN (Table 3). All calculations were carried out at 300 K.

**Table 2.** Material properties used for the calculation of  $TBR_{eff}$  for different diamond-GaN interlayers.

	Bulk Thermal Conductivity ( $W m^{-1} K^{-1}$ )	Specific Heat ( $J Kg^{-1} K^{-1}$ )	Density ( $Kg m^{-3}$ )	Average Phonon Group Velocity ( $m s^{-1}$ )	Debye Temperature (K)
Diamond	N/A	N/A	3515 <sup>28</sup>	$14.4 \times 10^3$	1860 <sup>40</sup>
GaN	130	490	6150	$5.4 \times 10^3$	600
AlN	285	600	3230	$7.8 \times 10^3$	1150
6H-SiC	490	690	3210	$9.1 \times 10^3$	1200

Unless specified, properties retrieved from the NSM database.

## RESULTS AND DISCUSSION

The structure and composition of the GaN-on-Si wafer prior to etching and diamond growth are shown in fig. 2. These show an 18 nm thick buried AlGaN interlayer below the 750 nm AlGaN/GaN channel with an Al content approximately 32%, determined by EDS from the Al rich region of the bottom of the layer.

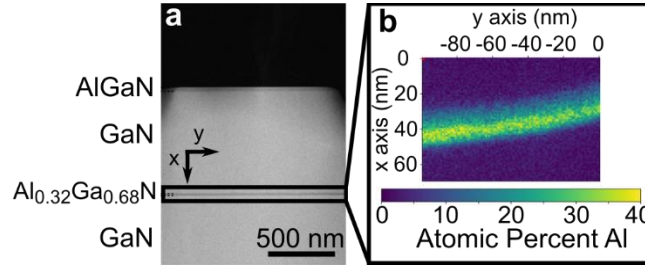


**Figure 2.** TEM image of the initial stack (a). EDS map of the AlGaN interlayer (b).

Following etching and diamond growth, further TEM characterization was performed on sample 2 (Fig. 3). Fig. 3a shows a TEM image of Sample 2 following etching and diamond growth. The area of the interface in Fig 3a, highlighted in red was investigated using EDS, with the results shown in Fig 3c.

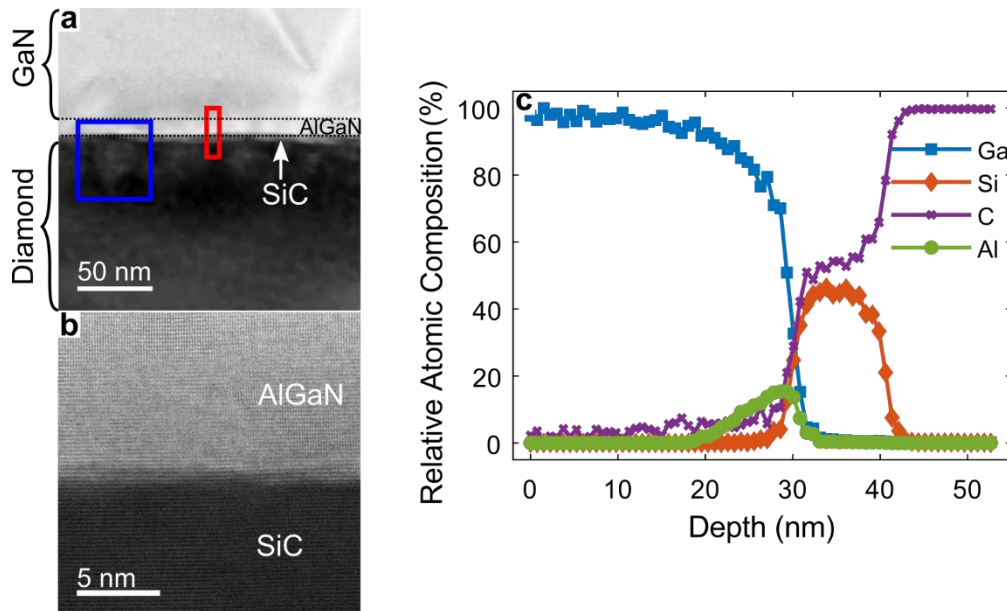


**Figure 3.** TEM micrographs of the GaN/AlGaN/SiC/diamond sample (Sample 2). Panel **a** is an image of the diamond-GaN interface, a diamond seed is highlighted in blue and a seedless area in red. A SiC interlayer with lighter contrast, arrowed, can be seen between the diamond and the AlGaN. Panel **b** shows an atomic resolution STEM image of the AlGaN-SiC interface. Panel **c** shows an EDS line scan taken from the area highlighted in red in panel **a** showing GaN, AlGaN, SiC, and diamond layers.

The scan shows that the selective etch successfully stopped on the AlGaN etch stop layer, indicated by a spike in the Al content approximately 15 nm thick. The slight ~5 nm thickness decrease of this layer is likely due to unintended etching during the selective RIE and diamond growth. The EDS also confirms the presence of a 10 nm thick SiC layer, apparent in Fig. 3b as areas with lighter contrast than the diamond. High resolution STEM indicates that the SiC/AlGaN interface is crystalline (Fig. 3b). Further high-resolution STEM of the structure and fast Fourier transforms of the images show that the SiC interlayer is hexagonal phase, either 2H or 6H SiC (Fig. 4). In comparison, the interface of sample 1 after etching and diamond growth is shown in Fig. 5a. The EDS scans (Fig. 5b and c) show that etch successfully stopped on the AlGaN etch stop and that no SiC is present. Note that although the Al content of the AlGaN layer appears to be lower for sample 1, this is relative to total composition and the two samples have very similar Al to Ga ratios of ~25% Al at the diamond interface. The lowering compared to the as-grown wafer (32%) may be a result of measurement error, small composition variation across the wafer, and slight etching of the Al rich bottom region of the layer during the ICP etch. The AlGaN layer is

pitted resulting in small voids at the interface with the diamond. This is likely induced by the harsh diamond growth conditions in a manner seen previously with GaN and SiN<sub>x</sub><sup>15</sup>.

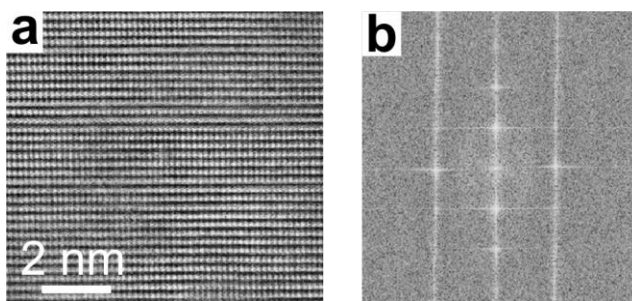


**Figure 4.** Atomic resolution STEM image of the SiC layer between the AlGaN and diamond in Sample 2 (a) and Fast Fourier transform consistent hexagonal-SiC (b).

We propose that the SiC layer forms during diamond growth: the surrounding Si substrate is sputtered onto the AlGaN when exposed to the microwave plasma before reacting with the carbon species present in the plasma. This is enabled by the low diamond seeding density – a result of the use of oxygen terminated nanodiamond seeds as opposed to hydrogen terminated seeds<sup>16</sup> and the use of drop casting rather than conventional ultrasonic seeding methods. We note that with a high seeding density, the nanodiamond seeds would obstruct deposition of the Si layer on the AlGaN, preventing SiC formation at this interface. This theory is supported by the area highlighted in blue in Fig. 3a. Electron energy loss spectroscopy shows a high sp<sup>2</sup> carbon content here (see supporting information), consistent with a nanodiamond seed layer, the outline of which can be seen in the micrograph. This seed layer is very close to the AlGaN with little SiC apparent between the two, consistent with the SiC forming after nanodiamond deposition and thus during diamond growth. Formation of crystalline SiC during MWCVD diamond growth is not a new phenomenon and has been reported for diamond growth on a Si substrate<sup>41</sup>. Whilst the SiC forming in this work is a result of the membrane fabrication technique, it is possible to

form crystalline SiC layers in the MWCVD reactor before diamond growth by the introduction of Si containing gases to the reactor<sup>42</sup>.

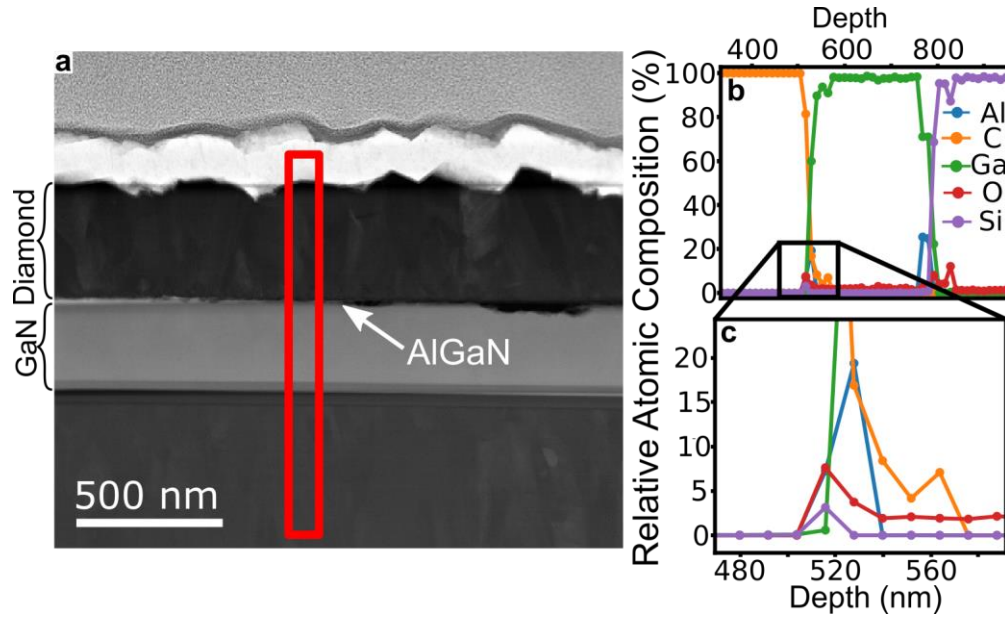


**Figure 5.** TEM micrograph, **a**, and EDS scans, **b** & **c**, of sample 1's diamond-GaN interface. Panel **c** shows the boxed section of **b** magnified. The EDS scan was taken from the area highlighted with the red box in panel **a**.

Fig. 6a shows representative TTR traces for both samples. The different appearance arises because of differences in the layer structure between the two samples (Fig. 1). Sensitivity analyses of the fitting parameters used for Sample 1 and 2 are shown in Figs. 6b and 6c respectively. The sensitivity to a parameter,  $\zeta$ , is defined as  $S_{\zeta} = \frac{\partial \ln R}{\partial \ln \zeta}$  where  $R$  is the measured thermoreflectance trace<sup>43</sup>. These graphs show that the fitting parameters have peak sensitivities at different times, i.e. they have sufficient independence for accuracy. Note, the diamond thickness was fitted for sample 1 due to variations across the film of ~300 nm. Whilst TEM confirms the film is ~500 nm thick in one location (Fig. 5a), some variation of thickness occurred across the sample.

The thermal conductivity of polycrystalline diamond varies throughout the layer's thickness, increasing further away from the nucleation interface as the grain size increases<sup>44,45</sup>. To allow for a direct comparison between samples with different diamond thicknesses, the following procedure was used; the thermal conductivity of the thin diamond film of Sample 1 was fixed using the calculations reported by Anaya *et al.*<sup>13</sup>. This thermal conductivity value was then used for the first 1  $\mu\text{m}$  of the nucleation interface of Sample 2, and the remaining bulk of the diamond layer fixed at a higher value. These values are described as “Diamond Near Nucleation Layer” and “Diamond Bulk” respectively in Table 1. Additionally, the anisotropic thermal conductivity of the polycrystalline diamond was included in the analysis, based on the model reported by Anaya *et al.*<sup>13</sup>.

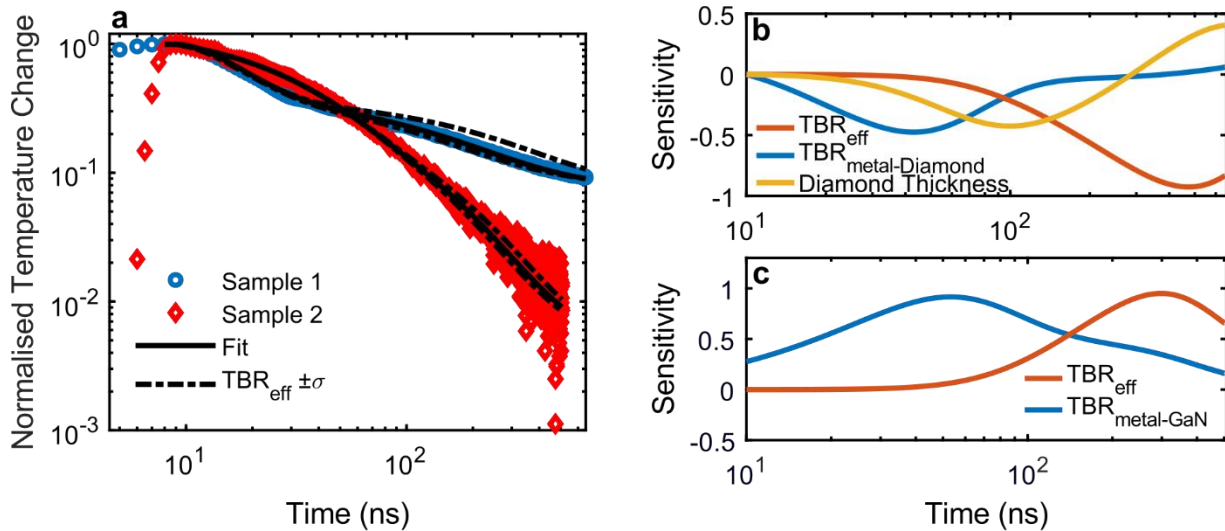


**Figure 6.** Panel **a** shows representative measured TTR traces for GaN/AlGaIn/diamond (Sample 1) and GaN/AlGaIn/SiC/diamond (Sample 2). The solid lines show the fit for these traces whilst the dotted lines show fits using one plus/minus standard deviation from the mean  $TBR_{\text{eff}}$ . Panels **b** and **c** show sensitivity analyses for the fitted parameters for Samples 1 and 2.

Table 3 shows the parameters obtained from the TTR fitting. Sample 2, with the SiC layer, had a  $TBR_{\text{eff}}$  of  $30 \pm 5 \text{ m}^2 \text{ K GW}^{-1}$  which is significantly lower than the  $104 \pm 44 \text{ m}^2 \text{ K GW}^{-1}$  value of

Sample 1. The larger error bar in the fitted  $TBR_{\text{eff}}$  of Sample 1 reflects some material variation across the sample surface. The SiC layer evidently improves heat transport across the  $\text{Al}_{0.32}\text{Ga}_{0.68}\text{N}$ /diamond interface. Waller *et al.* have shown that a low  $TBR_{\text{eff}}$  can only be achieved for a well bonded interface, with weakly bonded (van der Waals) interfaces acting as a low pass acoustic filter<sup>46</sup>. GaN does not readily form a carbide bond, resulting in poor adhesion to diamond, whereas AlN is known to form a strong carbide bond resulting in good adhesion to diamond<sup>16,19</sup>. It remains to be seen what the Al compositional threshold is at which AlGaN forms a strong carbide bond to diamond. For the  $\text{Al}_{0.32}\text{Ga}_{0.68}\text{N}$  considered here, the lower  $TBR_{\text{eff}}$  of Sample 2 (AlGaN/SiC/diamond) compared to Sample 1 (AlGaN/diamond) suggests that for these compositions there is a benefit to include a SiC interlayer which promotes adhesion between the AlGaN and diamond, therefore improving heat transport. For pure AlN or high Al content AlGaN, it is unlikely the SiC would be needed.

**Table 3.** Mean values of fitted parameters from TTR traces.

	$TBR_{\text{metal}} (\text{m}^2 \text{ K GW}^{-1})$	$TBR_{\text{eff}} (\text{m}^2 \text{ K GW}^{-1})$	Diamond Thickness (nm)
Sample 1	$74 \pm 13$	$107 \pm 44$	$643 \pm 85$
Sample 2	$71 \pm 7$	$30 \pm 5$	Not Fitted

Error bars from standard deviation obtained from multiple fitted traces

Simulation results of the contribution of the interlayer  $TBR_{\text{eff}}$ , called here  $TBR_{\text{interlayer}}$ , are shown in Fig. 7a when using an interlayer of only AlN, SiC, or  $\text{Al}_{0.32}\text{Ga}_{0.68}\text{N}$ , at a variety of different thicknesses. In all cases, the theoretical minimum  $TBR_{\text{interlayer}}$  is very small,  $< 4 \text{ m}^2 \text{ K GW}^{-1}$  for  $\text{Al}_{0.32}\text{Ga}_{0.68}\text{N}$  and  $< 2 \text{ m}^2 \text{ K GW}^{-1}$  for both SiC and AlN. Whilst these numbers are likely beyond the practical limit, it does illustrate that there is room for optimization of the experimental structures discussed earlier. The higher limiting value for  $\text{Al}_{0.32}\text{Ga}_{0.68}\text{N}$  is a result of its much lower

Debye temperature than diamond, indicating a poorer overlap of phonon density of states compared to both AlN and SiC<sup>47–49</sup>. This results in an increased TBR at the diamond interface. Additionally, the thermal conductivity of the Al<sub>0.32</sub>Ga<sub>0.68</sub>N is considerably lower than either SiC or AlN due to alloy scattering, resulting in a more prominent dependence on the thickness of the interlayer. This can be seen in fig. 7a as the TBR<sub>interlayer</sub> value does not begin to plateau until the thickness is below 10 nm whereas, for both AlN and SiC, the thickness dependence of TBR<sub>interlayer</sub> is minimal with the limiting value being reached at ~30 nm. For AlN, the predicted TBR<sub>interlayer</sub> is somewhat lower than experimentally reported value of 16 m<sup>2</sup> K GW<sup>-1</sup> for diamond on AlN seed layers<sup>16</sup>. This is likely due to the assumptions outlined earlier as well as a slight overprediction of the thin film AlN thermal conductivity in this model.

The effect of Al composition on the calculated TBR<sub>interlayer</sub> for a 20 nm thick interlayer is examined in fig. 7b. Here, the total TBR<sub>interlayer</sub> is plotted alongside its constituent terms: the interlayers' thermal resistance (AlGa<sub>x</sub>N Film) and the combined resistance of the TBRs of the two interfaces (TBR<sub>DMM</sub>). This graph shows how important a high Al composition is in reducing the theoretical TBR<sub>interlayer</sub>. As the alloy becomes more AlN like, TBR<sub>DMM</sub> is reduced due to increased phonon density of states overlap with the diamond and more similar Debye temperature (Table 3)<sup>48,50</sup>. Additionally, the film resistance is reduced as the thermal conductivity of the layer begins to increase sharply beyond 60% Al. Hence, the benefit of a high Al content AlGa<sub>x</sub>N interlayer is two-fold; first, higher Al content reduces TBR<sub>interlayer</sub> and, second, Al aids carbide formation and, the formation of a good thermal interface with the diamond. The calculated TBR<sub>interlayer</sub> values for AlN and SiC, and high Al (>60%) containing AlGa<sub>x</sub>N compare very favorably to one of the lowest TBR<sub>eff</sub> values of 9.5(+3.9/-1.7) m<sup>2</sup> K GW<sup>-1</sup> measured for a 5 nm thick SiN<sub>x</sub> interlayer<sup>51</sup>. Whilst the calculated values are at the lower limit of what is experimentally achievable, one advantage of

the crystalline interlayers is that low  $TBR_{\text{eff}}$  values can be achieved with considerably thicker interlayers. If the interlayer is too thin it will not offer the necessary protection to the GaN during diamond growth, resulting in pinholes forming and propagating through the GaN. These defects are highly detrimental for device performance<sup>15</sup>. The experimental work shown here indicates that the thin SiC layer is relatively stable during diamond growth with no evidence of significant etching, meaning it could offer better protection than  $\text{SiN}_x$ . However, the low Al content AlGaN appears to be readily etched and may suffer from similar issues to the  $\text{SiN}_x$  layers.

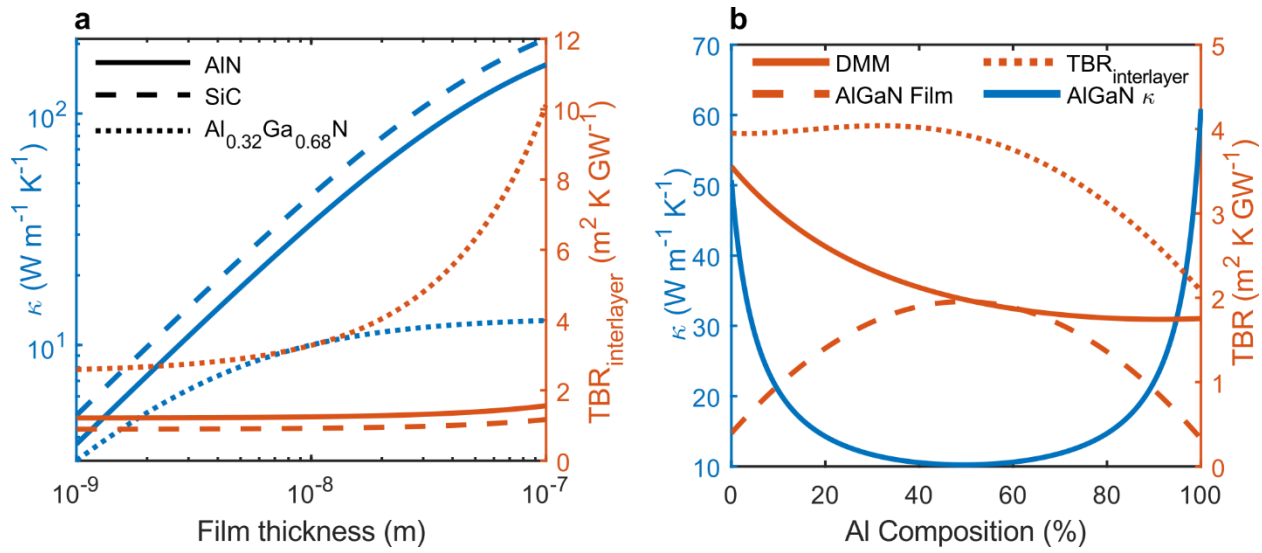


**Figure 7.** In panel **a**, the left axis shows the calculated thermal conductivity of SiC, AlN, and  $\text{Al}_{0.32}\text{Ga}_{0.68}\text{N}$  for different thicknesses calculated using the grey approximation. The right axis shows the calculated  $TBR_{\text{interlayer}}$  using the different interlayers, combining the thermal resistance of the layer with the calculated fundamental thermal boundary resistance using the diffuse mismatch model. Panel **b** shows the same calculations but as a function of Al composition for a 20 nm thick AlGaN interlayer. The contributions to  $TBR_{\text{interlayer}}$  of the film (AlGaN Film) and the interfaces ( $TBR_{\text{DMM}}$ ) are shown.

## CONCLUSIONS

Diamond has been grown directly onto an  $\text{Al}_{0.32}\text{Ga}_{0.68}\text{N}$  interlayer integrated into a GaN/AlGaN device epitaxy. For low Al content AlGaN interlayers it is shown to be advantageous to include a SiC layer, which improves heat transport from the GaN into the diamond to achieve a low  $\text{TBR}_{\text{eff}}$  ( $30 \pm 5 \text{ m}^2 \text{ K GW}^{-1}$ ), similar to the state-of-the art for  $\text{SiN}_x$  interlayers of similar thickness. This SiC layer is likely to increase the bond strength between the diamond and the GaN structure due to increased carbide bonding. Calculations predict that single crystal SiC and AlN interlayers could enable extremely low  $\text{TBR}_{\text{eff}}$  values, with the predicted lower limit these layers contribute being less than  $2 \text{ m}^2 \text{ K GW}^{-1}$ .  $\text{Al}_x\text{Ga}_{(1-x)}\text{N}$  interlayers could also offer a route to low  $\text{TBR}_{\text{eff}}$  values ( $< 5 \text{ m}^2 \text{ K GW}^{-1}$ ) particularly with high Al content ( $>60\%$ ).

## SUPPORTING INFORMATION

EELS and TEM images of nanodiamond seed (PDF)

## ACKNOWLEDGEMENTS

The authors would like to acknowledge financial support from the Engineering and Physical Sciences Research Council (EPSRC) under the program Grant GaN-DaME (Grant No. EP/P00945X/1). D.Field's PhD studentship is co-funded by the EPSRC Centre for Doctoral Training in Diamond Science & Technology (EP/L015315/1) and Element-Six Technologies. The authors would also like to acknowledge and thank D. Francis at Akash Systems for wafer bonding as well as R. Simon (TherMap Solutions) for useful discussion on experimental measurements and data analysis.

## REFERENCES

- 327 (1) Bar-Cohen, A.; Maurer, J. J.; Altman, D. H. Embedded Cooling for Wide Bandgap Power  
328 Amplifiers: A Review. *J. Electron. Packag.* **2019**, *141* (4), 1–14.  
329 <https://doi.org/10.1115/1.4043404>.
- 330 (2) Wu, Y. F.; Saxler, A.; Moore, M.; Smith, R. P.; Sheppard, S.; Chavarkar, P. M.; Wisleder,  
331 T.; Mishra, U. K.; Parikh, P. 30-W/Mm GaN HEMTs by Field Plate Optimization. *IEEE*  
332 *Electron Device Lett.* **2004**, *25* (3), 117–119. <https://doi.org/10.1109/LED.2003.822667>.
- 333 (3) Pomeroy, J. W.; Uren, M. J.; Lambert, B.; Kuball, M. Operating Channel Temperature in  
334 GaN HEMTs: DC versus RF Accelerated Life Testing. *Microelectron. Reliab.* **2015**, *55*  
335 (12), 2505–2510. <https://doi.org/10.1016/j.microrel.2015.09.025>.
- 336 (4) Bougrov, V.; Levinshtein, M. E.; Rumyantsev, S. L.; Zubrilov, A. *Properties of Advanced*  
337 *Semiconductor Materials GaN, AlN, InN, BN, SiC, SiGe*; 2001.
- 338 (5) Glassbrenner, C. J.; Slack, G. A. Thermal Conductivity of Silicon and Germanium from 3K  
339 to the Melting Point. *Phys. Rev.* **1964**, *134* (4A). [https://doi.org/10.1007/s11892-016-0785-](https://doi.org/10.1007/s11892-016-0785-8)  
340 8.
- 341 (6) Kurlov, V. N. Sapphire: Properties, Growth, and Applications. In *Encyclopedia of*  
342 *Materials: Science and Technology*; 2001; pp 8259–8264. [https://doi.org/10.1016/b0-08-](https://doi.org/10.1016/b0-08-043152-6/01478-9)  
343 043152-6/01478-9.
- 344 (7) Onn, D. G.; Witek, A.; Qiu, Y. Z.; Anthony, T. R.; Banholzer, W. F. Some Aspects of the  
345 Thermal Conductivity of Isotopically Enriched Diamond Single Crystals. *Phys. Rev. Lett.*  
346 **1992**, *68* (18), 2806–2809. <https://doi.org/10.1103/PhysRevLett.68.2806>.
- 347 (8) Zhou, Y.; Ramaneti, R.; Anaya, J.; Korneychuk, S.; Derluyn, J.; Sun, H.; Pomeroy, J.;

- 348 Verbeeck, J.; Haenen, K.; Kuball, M. Thermal Characterization of Polycrystalline Diamond  
 349 Thin Film Heat Spreaders Grown on GaN HEMTs. *Appl. Phys. Lett.* **2017**, *111* (4).  
 350 <https://doi.org/10.1063/1.4995407>.
- 351 (9) Hageman, P. R.; Schermer, J. J.; Larsen, P. K. GaN Growth on Single-Crystal Diamond  
 352 Substrates by Metalorganic Chemical Vapor Deposition and Hydride Vapour Deposition.  
 353 *Thin Solid Films* **2003**, *443* (1–2), 9–13. [https://doi.org/10.1016/S0040-6090\(03\)00906-4](https://doi.org/10.1016/S0040-6090(03)00906-4).
- 354 (10) Gerrer, T.; Cimalla, V.; Waltereit, P.; Müller, S.; Benkhelifa, F.; Maier, T.; Czap, H.;  
 355 Ambacher, O.; Quay, R. Transfer of AlGaN/GaN RF-Devices onto Diamond Substrates via  
 356 van Der Waals Bonding. *Proc. Int. Astron. Union* **2018**, *10* (5–6), 666–673.  
 357 <https://doi.org/10.1017/S1759078718000582>.
- 358 (11) Pomeroy, J. W.; Bernardoni, M.; Dumka, D. C.; Fanning, D. M.; Kuball, M. Low Thermal  
 359 Resistance GaN-on-Diamond Transistors Characterized by Three-Dimensional Raman  
 360 Thermography Mapping. *Appl. Phys. Lett.* **2014**, *104* (8).  
 361 <https://doi.org/10.1063/1.4865583>.
- 362 (12) Francis, D.; Faili, F.; Babić, D.; Ejeckam, F.; Nurmikko, A.; Maris, H. Formation and  
 363 Characterization of 4-Inch GaN-on-Diamond Substrates. *Diam. Relat. Mater.* **2010**, *19* (2–  
 364 3), 229–233. <https://doi.org/10.1016/j.diamond.2009.08.017>.
- 365 (13) Anaya, J.; Sun, H.; Pomeroy, J.; Kuball, M. Thermal Management of GaN-on-Diamond  
 366 High Electron Mobility Transistors: Effect of the Nanostructure in the Diamond near  
 367 Nucleation Region. *Proc. 15th Intersoc. Conf. Therm. Thermomechanical Phenom.*  
 368 *Electron. Syst. ITherm 2016* **2016**, 1558–1565.  
 369 <https://doi.org/10.1109/ITHERM.2016.7517734>.

- 370 (14) Kaloyeros, A. E.; Jové, F. A.; Goff, J.; Arkles, B. Review—Silicon Nitride and Silicon  
371 Nitride-Rich Thin Film Technologies: Trends in Deposition Techniques and Related  
372 Applications. *ECS J. Solid State Sci. Technol.* **2017**, *6* (10), P691–P714.  
373 <https://doi.org/10.1149/2.0011710jss>.
- 374 (15) Liu, D.; Francis, D.; Faili, F.; Middleton, C.; Anaya, J.; Pomeroy, J. W.; Twitchen, D. J.;  
375 Kuball, M. Impact of Diamond Seeding on the Microstructural Properties and Thermal  
376 Stability of GaN-on-Diamond Wafers for High-Power Electronic Devices. *Scr. Mater.*  
377 **2017**, *128*, 57–60. <https://doi.org/10.1016/j.scriptamat.2016.10.006>.
- 378 (16) Mandal, S.; Yuan, C.; Massabuau, F.; Pomeroy, J. W.; Cuenca, J.; Bland, H.; Thomas, E.;  
379 Wallis, D.; Batten, T.; Morgan, D.; Oliver, R.; Kuball, M.; Williams, O. A. Thick , Adherent  
380 Diamond Films on AlN with Low Thermal Barrier Resistance. *ACS Appl. Mater. Interfaces*  
381 **2019**. <https://doi.org/10.1021/acsami.9b13869>.
- 382 (17) Sun, H.; Simon, R. B.; Pomeroy, J. W.; Francis, D.; Faili, F.; Twitchen, D. J.; Kuball, M.  
383 Reducing GaN-on-Diamond Interfacial Thermal Resistance for High Power Transistor  
384 Applications. *Appl. Phys. Lett.* **2015**, *106* (11). <https://doi.org/10.1063/1.4913430>.
- 385 (18) Slack, G. A.; Tanzilli, R. A.; Pohl, R. O.; Vandersande, J. W. The Intrinsic Thermal  
386 Conductivity of AlN. *J. Phys. Chem. Solids* **1987**, *48* (7), 641–647.
- 387 (19) May, P. W.; Tsai, H. Y.; Wang, W. N.; Smith, J. A. Deposition of CVD Diamond onto GaN.  
388 *Diam. Relat. Mater.* **2006**, *15* (4–8), 526–530.  
389 <https://doi.org/10.1016/j.diamond.2005.11.036>.
- 390 (20) Kuball, M.; Pomeroy, J. W.; Uren, M. J.; Williams, O. A. UK Patent No. GB 1814192.9,

2019.

- (21) Smith, M. D.; Li, X.; Uren, M. J.; Thayne, I. G.; Kuball, M. Polarity Dependence in Cl<sub>2</sub>-Based Plasma Etching of GaN, AlGa<sub>N</sub> and AlN. *Appl. Surf. Sci.* **2020**, *521* (December 2019). <https://doi.org/10.1016/j.apsusc.2020.146297>.
- (22) Babic, D.; Clara, S.; Francis, D.; Diduck, Q.; Ejeckam, F. GALLUM-NITRIDE-ON-DIAMOND WAFERS AND DEVICES, AND METHODS OF MANUFACTURE. US 2014/0141595 A1, 2014.
- (23) Smith, M. D.; Cuenca, J. A.; Field, D. E.; Fu, Y.; Yuan, C.; Oliver, R. A.; Kuball, M.; Mandal, S.; Pomeroy, J. W.; Thayne, I.; Uren, M. J.; Williams, O. A.; Smith, M. D.; Cuenca, J. A.; Pomeroy, J. W.; Williams, O. A. GaN-on-Diamond Technology Platform : Bonding-Free Membrane Manufacturing Process GaN-on-Diamond Technology Platform : Bonding-Free Membrane Manufacturing Process. *AIP Adv.* **2020**, *10* (3), 1–6. <https://doi.org/10.1063/1.5129229>.
- (24) Han, Y.; Xue, S.; Guo, W.; Luo, Y.; Hao, Z.; Sun, C. Highly Selective Dry Etching of GaN over AlGa<sub>N</sub> Using Inductively Coupled Cl<sub>2</sub>/N<sub>2</sub>/O<sub>2</sub> Plasmas. *Japanese J. Appl. Physics, Part 2 Lett.* **2003**, *42* (10 A), 8–11. <https://doi.org/10.1143/jjap.42.11139>.
- (25) Yuan, C.; Pomeroy, J. W.; Kuball, M. Above Bandgap Thermoreflectance for Non-Invasive Thermal Characterization of GaN-Based Wafers. *Appl. Phys. Lett.* **2018**, *113* (102101). <https://doi.org/10.1063/1.5040100>.
- (26) Zhou, Y.; Anaya, J.; Pomeroy, J.; Sun, H.; Gu, X.; Xie, A.; Beam, E.; Becker, M.; Grotjohn, T. A.; Lee, C.; Kuball, M. Barrier-Layer Optimization for Enhanced GaN-on-Diamond

- 412 Device Cooling. *ACS Appl. Mater. Interfaces* **2017**, 9 (39), 34416–34422.  
413 <https://doi.org/10.1021/acsami.7b08961>.
- 414 (27) Chen, G.; Hui, P. Thermal Conductivities of Evaporated Gold Films on Silicon and Glass.  
415 *Appl. Phys. Lett.* **1999**, 74 (20), 2942–2944. <https://doi.org/10.1063/1.123973>.
- 416 (28) Haynes, W. M.; Lide, D. R. *CRC Handbook of Chemistry and Physics*, 92nd ed.; CRC ;  
417 Boca Raton, Fla., 2011.
- 418 (29) Sichel, E. K.; Pankove, J. I. Thermal Conductivity of GaN, 25–360 K. *J. Phys. Chem. Solids*  
419 **1977**, 38 (3), 330.
- 420 (30) Levinshtein, M. E.; Rumyantsev, S. L.; Shur, M. S. *Properties of Advanced Semiconductor*  
421 *Materials: GaN, AlN, InN, BN, SiC, SiGe*; John Wiley & Sons, 2001.
- 422 (31) DeSorbo, W. Specific Heat of Diamond at Low Temperatures. *J. Chem. Phys.* **1953**, 21 (5),  
423 876–880.
- 424 (32) Liebchen, R.; Breitschädel, O.; Durmaz, A. R.; Griesinger, A. Thermal Characterization of  
425 Epitaxial Grown Polycrystalline Silicon. *Thin Solid Films* **2016**, 606, 99–105.  
426 <https://doi.org/10.1016/j.tsf.2016.03.030>.
- 427 (33) Ozevin, D. *Micro-Electro-Mechanical-Systems (MEMS) for Assessing and Monitoring*  
428 *Civil Infrastructures*; 2014; Vol. 1. <https://doi.org/10.1533/9780857099136.265>.
- 429 (34) Okhotin, A. S.; Pushkarskii, A. S.; Gorbachev, V. Thermophysical Properties of  
430 Semiconductors, Atom Publ. *Atom Publ. House* **1972**.
- 431 (35) Grove, A. S. *Physics and Technology of Semiconductor Devices*; Wiley: New York, 1967.

- 432 (36) McGaughey, A. J. H.; Landry, E. S.; Sellan, D. P.; Amon, C. H. Size-Dependent Model for  
433 Thin Film and Nanowire Thermal Conductivity. *Appl. Phys. Lett.* **2011**, *99* (131904).  
434 <https://doi.org/10.1063/1.3644163>.
- 435 (37) Majumdar, A. Microscale Heat Conduction in Dielectric Thin Films. *J. Heat Transfer* **1993**,  
436 *115* (1), 7–16. <https://doi.org/10.1115/1.2910673>.
- 437 (38) Szymański, M. Calculation of the Cross-Plane Thermal Conductivity of a Quantum Cascade  
438 Laser Active Region. *J. Phys. D. Appl. Phys.* **2011**, *44* (8). [https://doi.org/10.1088/0022-](https://doi.org/10.1088/0022-3727/44/8/085101)  
439 [3727/44/8/085101](https://doi.org/10.1088/0022-3727/44/8/085101).
- 440 (39) Adachi, S. III-V Ternary and Quaternary Compounds. In *Springer Handbook of Electronic*  
441 *and Photonic Materials*; Kasap, S., Capper, P., Eds.; Springer International Publishing:  
442 Cham, 2017; p 1. [https://doi.org/10.1007/978-3-319-48933-9\\_30](https://doi.org/10.1007/978-3-319-48933-9_30).
- 443 (40) Ashcroft, N. W.; Mermin, N. D. *Solid State Physics*, 1st ed.; Crane, D. G., Ed.; Holt,  
444 Rinehart and Winston, 1976.
- 445 (41) Je, J. H.; Noh, D. Y. Microstructure of Diamond and  $\beta$ -SiC Interlayer Studied by  
446 Synchrotron x-Ray Scattering. *J. Appl. Phys.* **1996**, *80* (5), 2791–2798.  
447 <https://doi.org/10.1063/1.363197>.
- 448 (42) Sedov, V. S.; Martyanov, A. K.; Khomich, A. A.; Savin, S. S.; Voronov, V. V.;  
449 Khmelnitskiy, R. A.; Bolshakov, A. P.; Ralchenko, V. G. Co-Deposition of Diamond and  
450  $\beta$ -SiC by Microwave Plasma CVD in H<sub>2</sub>-CH<sub>4</sub>-SiH<sub>4</sub> Gas Mixtures. *Diam. Relat. Mater.*  
451 **2019**, *98* (July). <https://doi.org/10.1016/j.diamond.2019.107520>.
- 452 (43) Jiang, P.; Qian, X.; Yang, R. Tutorial: Time-Domain Thermoreflectance (TDTR) for

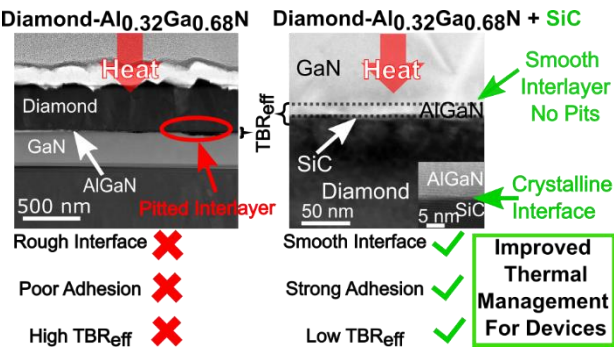
- 453 Thermal Property Characterization of Bulk and Thin Film Materials. *J. Appl. Phys.* **2018**,  
454 *124* (16). <https://doi.org/10.1063/1.5046944>.
- 455 (44) Spiteri, D.; Anaya, J.; Kuball, M. The Effects of Grain Size and Grain Boundary  
456 Characteristics on the Thermal Conductivity of Nanocrystalline Diamond. *J. Appl. Phys.*  
457 **2016**, *119*, 085102. <https://doi.org/10.1063/1.4942522>.
- 458 (45) Anaya, J.; Simon, R. B.; Balmer, R.; Twitchen, D. J.; Faili, F.; Kuball, M.; Williams, G. T.  
459 Effect of Grain Size of Polycrystalline Diamond on Its Heat Spreading Properties. *Appl.*  
460 *Phys. Express* **2016**, *9* (6), 061302. <https://doi.org/10.7567/apex.9.061302>.
- 461 (46) Waller, W. M.; Pomeroy, J. W.; Field, D. E.; Smith, E. J. W.; May, P. W.; Martin, K.  
462 Thermal Boundary Resistance of Direct van Der Waals Bonded GaN-on-Diamond.  
463 *Semicond. Sci. Technol.*
- 464 (47) Protik, N. H.; Katre, A.; Lindsay, L.; Carrete, J.; Mingo, N.; Broido, D. Phonon Thermal  
465 Transport in 2H, 4H and 6H Silicon Carbide from First Principles. *Mater. Today Phys.* **2017**,  
466 *1*, 31–38. <https://doi.org/10.1016/j.mtphys.2017.05.004>.
- 467 (48) Mounet, N.; Marzari, N. First-Principles Determination of the Structural, Vibrational and  
468 Thermodynamic Properties of Diamond, Graphite, and Derivatives. *Phys. Rev. B - Condens.*  
469 *Matter Mater. Phys.* **2005**, *71* (20), 1–14. <https://doi.org/10.1103/PhysRevB.71.205214>.
- 470 (49) Davydov, V. Y.; Kitaev, Y. E.; Goncharuk, I. N.; Smirnov, A. N. Phonon Dispersion and  
471 Raman Scattering in Hexagonal GaN and AlN. *Phys. Rev. B* **1998**, *58* (19), 12 899–12 907.
- 472 (50) Bungaro, C.; Rapcewicz, K.; Bernholc, J. Ab Initio Phonon Dispersions of Wurtzite AlN,  
473 GaN, and InN. *Phys. Rev. B - Condens. Matter Mater. Phys.* **2000**, *61* (10), 6720–6725.

474 <https://doi.org/10.1103/PhysRevB.61.6720>.

475 (51) Yates, L.; Anderson, J.; Gu, X.; Lee, C.; Bai, T.; Mecklenburg, M.; Aoki, T.; Goorsky, M.  
476 S.; Kuball, M.; Piner, E. L.; Graham, S. Low Thermal Boundary Resistance Interfaces for  
477 GaN-on-Diamond Devices. *ACS Appl. Mater. Interfaces* **2018**, *10* (28), 24302–24309.  
478 <https://doi.org/10.1021/acsami.8b07014>.

479

480 For Table of Contents Only



481